Water-mediated optical and morphological tuning of highly stable orange-emitting Mn-doped perovskite for white light-emission

Sangeun Cho[1], Vijaya Gopalan Sree[1], Akash V. Fulari[1], Sanghyuk Park[2,3], Ming Mei[2], Minju Kim[2], Atanu Jana[1], Deblina Das[1], Hyunsik Im[1], Kwangseuk Kyhm[2], Robert A. Taylor[3]

[1] Division of Physics and Semiconductor Science, Dongguk University, Seoul 04620, South Korea.

[2] Department of Opto-mechatronics Engineering, RCDAMP, Pusan National University, Busan 46241, South Korea

[3] Clarendon Laboratory, Department of Physics, University of Oxford, Parks Road, Oxford OX1 3PU, UK

[+] Equally contributed.

Corresponding authors: kskyhm@pusan.ac.kr; hyunsik7@dongguk.edu

Abstract

The main challenges in the optical and morphological tuning of highly stable orange-emitting Mn-doped perovskite include achieving uniform dopant distribution, maintaining structural integrity under varying environmental conditions, and optimizing luminescent efficiency while minimizing non-radiative recombination pathways. This study presents a novel, one-step, water-induced ultrafast synthesis strategy for obtaining Mn-doped mixed-halide perovskites at room temperature. This technique offers morphological control by varying the amount of water-based precursor, allowing the tuning of resulting nanostructures to produce nanoplatelets, nanocubes, or nanowires. In the growth mechanism, Mn^{2+} dopants affect the crystal structure by promoting stable growth and uniform doping at higher concentrations, while water improves ion dispersion, reaction

kinetics, and passivation, facilitating optimal crystal growth and the formation of desired nanostructure morphologies. The synthesized Mn:$CsPbBr_{3-x}Cl_x$ NCs form a highly stable colloidal solution with approximately 100 % emission stability for up to one year under ambient conditions and retain 98.9 % of its photoluminescence after aging at 85 °C for 200 h. We also explore the PL mechanism in Mn:$CsPbBr_{3-x}Cl_x$ NCs, where temperature-dependent PL analysis reveals energy transfer from $CsPbBr_{3-x}Cl_x$exciton states to Mn^{2+}-doped levels, enhancing PL intensity, with both exciton and Mn^{2+}emissions exhibiting a blue shift as the temperature increased from 6 K to 300 K, attributed to lattice expansion and electron–phonon interactions. A warm white light emission is achieved with excellent stability and an exceptionally wide color gamut coverage. The proposed strategy has the potential to enable large-scale synthesis and fabrication of highly stable perovskite devices for high-quality display and lighting applications.

Keywords: Ligand-assisted reprecipitation, Nanostructured orange-emitting perovskite, Mn doping, High stability, Warm-white LED

Introduction

Lead halide perovskites (LHPs) have emerged as one of the most versatile materials of the decade[1]. In particular, their optical tunability via fast ion exchange reaction, size and shape control using various long and shorts chained ligands and their facile synthesis at room temperature (RT) have attracted attention of researchers working in the field of luminescent semiconductor nanocrystals (NCs)[2]. LHPs have shown great potential in applications such as light emitting diodes[3], solar cells[4], high energy radiation detectors[5], X-ray imagers[6], and light emitting memory devices etc.[7]

To improve and extend the usefulness of LHPs in these applications, their optical properties can be tuned using dopants [8]. For example, Manganese (Mn^{2+}) ions have been vastly employed and studied as dopants for improvement of photophysical properties of semiconductor nanocrystals[9,10,11,12,13,14,15]. Owing to their easy processability in solution form, introducing dopant ions into LHPs can result in excellent optoelectronic and magnetic properties as an effect of interaction between host and dopant lattice[16,17,18,19,20,21]. One of the popular usages of Mn^{2+} doped LHPs is functioning as a red phosphor in down-converted white light emitting diodes[22,23,24,25,26].

Despite these excellent optical properties, conventional colloidal LHPs have a major flaw-poor stability. Exposure to moisture or water can lead to the formation of defects and deteriorate their photophysical properties limiting their overall practicality[27]. Since the genesis of colloidal LHPs, their poor stability against moisture has always been a hot topic[28]. However, for some device fabrication techniques, it has recently been documented that moisture can play a positive role in the formation of LHPs films[29]. For example, a common method to protect LHPs against moisture is to coat them using silica shell by using silane coupling agents[30,31,32]. For optimum silica network growth, the silane coupling agent requires small number of H_2O molecules which can be acquired from air, or it could be absorbed from solvents like toluene / DMF[33].

Ligand assisted re-precipitation (LARP) is one of the most practiced techniques for the synthesis of LHPs at RT[34]. In this process, a saturated precursor solution containing halide salts and a specific quantity of ligands in a polar solvent such as dimethylformamide (DMF) is required. The desired amount of this precursor solution is then injected into a non-polar solvent such as toluene and hexane. Due to an adequate difference in polarity between solvents, upon injection of the precursor solution into non-polar solvent leads to supersaturation. This triggers crystallization via nucleation and growth of perovskite NCs. But owing to polarity differences between generally

used solvent and antisolvent (e.g., relative polarity: 0.386 for DMF and 0.099 for toluene), they are inter-miscible, hence precursors prepared in DMF can mix homogeneously with toluene and this adversely affects the quality of obtained LHPs by inducing surface defects.

To address this issue, we propose a non-volatile doping strategy by using H_2O. On the solvent polarity index, H_2O exhibits the highest relative polarity of 1.0.[35] In the present study, we intentionally use H_2O as a dopant precursor for the synthesis of Mn-doped LHPs. Because of the large difference in relative polarity between toluene and H_2O, they cannot intermix. However, as a result of self-ionization process, H_2O can strip OA and OAM ligands and help transform the LHPs while providing dopant Mn^{2+} ions. We investigate in detail the photophysical properties of the proposed H_2O-induced Mn^{2+}-doped LHP NCs. We further analyze the effect of hydrohalic acid treatment on the NCs with hydrochloric acid (HCl) and Hydrobromic acid (HBr) and investigate their stability and optical properties. We also confirm excellent thermal cycling and aging of Mn^{2+} doped perovskite NCs, and as a proof of applicability we demonstrate a warm white light emitting diode constructed using combination of stable Mn^{2+} doped perovskite sample from our synthesis along with green emitting dual-phase $Cs_4PbBr_6/CsPbBr_3@SiO_2$ NCs (DPNCs) synthesized as per our previous report.

Materials and methods

Materials

All chemicals were reagent grade and were used without further purification. DMF (N, N-Dimethylformamide, anhydrous, 99.8%), toluene (≥ 99.9%), Hydrobromic acid (HBr, ACS reagent, 48%), Hydrochloric acid (HCl, ACS reagent, 37%), 3-Aminopropyl triethoxysilane (APTES, 99%), tetramethyl orthosilicate (TMOS, 99%), cesium bromide (CsBr 99.9% trace

metals basis), lead (II) bromide ($PbBr_2 \geq 98\%$), Manganese (II) chloride tetrahydrate ($MnCl_2 \cdot 4H_2O$, Reagent Plus, $\geq 99\%$), were purchased from Sigma-Aldrich.

Precursor preparation

The process involved two precursors. Precursor X consisted of equimolar quantities (0.04 mmol) of the halide salts CsBr and $PbBr_2$ dissolved in 10 ml of DMF with 1 ml of OA and 0.5 ml of OAM. Precursor Y was prepared by dissolving $MnCl_2.4H_2O$ in DI water at a concentration of 1.98 g/ml.

Mn doped Perovskite synthesis

In the typical synthesis route, 1 ml of precursor X was injected into 10 ml of toluene under vigorous vortexing. Blue-emitting $CsPbBr_3$ nanoplatelets formed after ~5 s. This was named as Sample 0. For the synthesis of Mn-doped mixed-halide perovskites, precursor X (1 ml) and various quantities of precursor Y (20–100 μL) were injected into 10 ml of toluene under vigorous vortexing. Samples prepared with injection of 20 μL, 40 μL, 60 μL, 80 μL, and 100 μL were named as Sample 1, 2, 3, 4, and 5 respectively. Depending on the quantity of the injected Mn water-based precursor, the luminescence of the mixed-halide perovskites ranged from magenta to pinkish to bright orange. Vortexing at ~3400 rpm was used throughout the reaction process. The as-synthesized colloidal NC solutions were used for subsequent characterization.

Hydrohalic acid treatment

A specific quantity of HCl or HBr was added into the antisolvent prior to precursor injection. Next, the desired quantity of precursor Y followed by precursor X was added into the above solution under vigorous vortexing. After 15 seconds of vortexing a milky white coloured solution was observed under daylight. Now the vortexing was stopped, vial was sealed to prevent contact with additional moisture and kept undisturbed at ambient conditions. After 48 hours, a crystal-clear

liquid was seen with whitish substance sinking at the bottom. This crystal-clear liquid was carefully pipetted out into a separate container without disturbing the vial and stored for further use. To obtain phosphor powders, 160 µL of tetramethyl orthosilicate was added into 3 ml of as prepared NC solution and stirred at 200 RPM under ambient conditions. After 36 hours, white coloured phosphor powders were obtained.

DPNCs synthesis

Green-emitting DPNCs were synthesized as per our previous report. The reaction precursor solution and NCs were synthesized at RT (24 °C). Typically, an equimolar amount of CsBr (0.4 mmol) and $PbBr_2$ (0.4 mmol) was dissolved in 10 ml of DMF by shaking on a vortex for 30 min at room temperature to form a clear precursor solution. An aliquot (1 ml) of the prepared precursor solution was added into 0.7 ml of APTES. Next, 0.1 ml of this precursor was swiftly injected into a vial containing 10 ml of toluene, under vigorous vortexing. Green emission was observed in 85 seconds. This vial was kept at ambient condition for 12 hours. The product (DPNCs) was collected by centrifuging at 12000 rpm and dried at 60 °C under vacuum oven. Later, DPNCs were used as a green phosphor in WLED device fabrication.

LED fabrication

Mn-doped mixed-halide perovskites prepared with 20 µL of HCl were mixed with inert PS at a concentration of 80 mg/ml in toluene. 800 µL of this solution was dried in a petri dish to form gel like consistency to be used as an orange-red active material. The as synthesized green emitting DPNCs powder were mixed with CPS 1040 UV curing polymer at 0.6:1 ratio. Both active materials were coated on a 400 nm UV chip simultaneously and let dry to produce warm white

LED. For thermal photostability tests, Mn doped sample powder mixed with UV curable resin was dropped in a petri dish, cured, and used.

Characterization

The powder X-ray diffraction (XRD) was performed on a Rigaku Ultima IV X-ray Diffractometer at 40 kV using Cu Ka radiation (k = 1.5406 Å). The Fourier-transform infrared spectroscopy (FTIR) analysis was carried out on Thermo-Scientific Nicolet 6700 / Nicolet iS50. The UV–vis measurements were performed using Jasco V-760 spectrophotometer. PL spectra were recorded using Thor Labs-OSA spectrofluorometer. The absolute PLQY measurements were performed using Jasco FP-8500 spectrofluorometer with an integrating sphere. The scanning electron microscope (SEM) analyses were carried out on HITACHI S-3000 N. The High-resolution TEM (HR-TEM) and energy-dispersive X-ray spectroscopy (EDS) analyses were carried out on a JEOL JEM-2200FS TEM. LED device were characterized using a Keithley 2635A source meter and a CS2000 spectroradiometer (Konica Minolta).

Results and Discussion

Figure 1a present a schematic illustration of the synthetic process used to obtain the Mn-doped mixed-halide perovskites. Precursors X and Y were injected into toluene under vigorous vortexing. When only precursor X was used, blue-emitting $CsPbBr_3$ nanoplatelets were obtained.

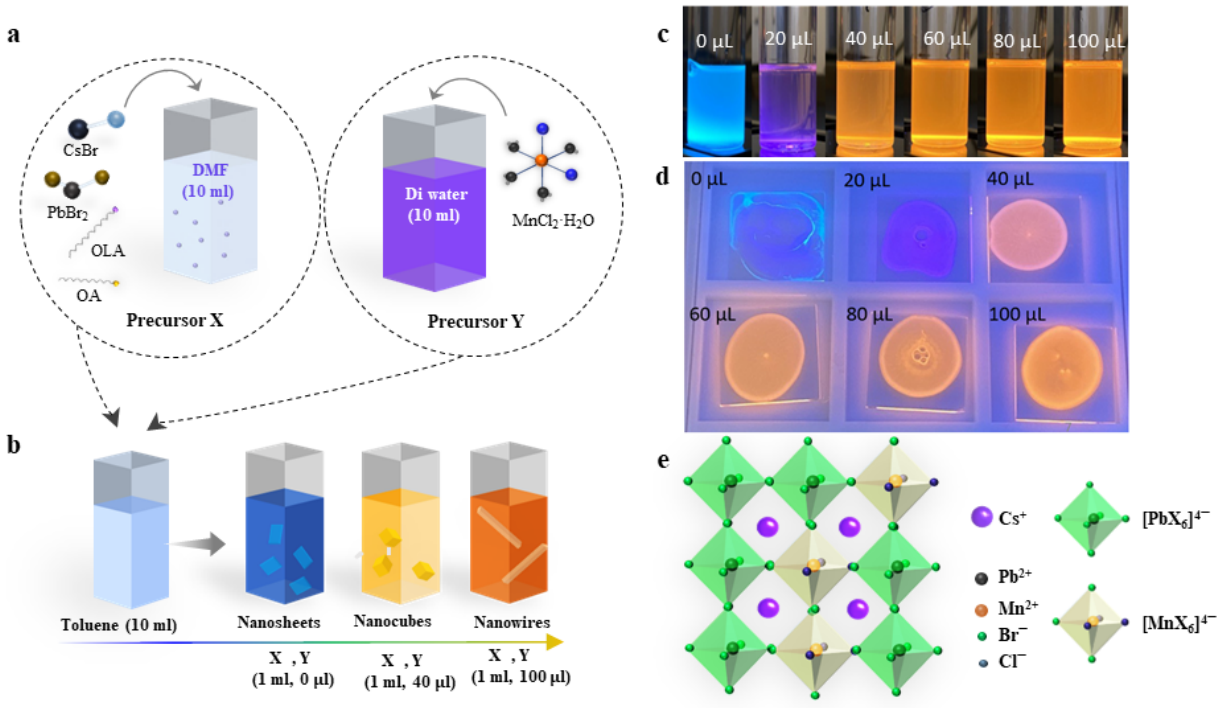

Fig. 1 Schematic illustration of the synthesis process for Mn-doped mixed-halide perovskites. **a** Clear precursor X was obtained by dissolving equimolar quantities of halide salts in DMF, while precursor Y was prepared by dissolving $MnCl_2.4H_2O$ in DI water. **b** Perovskite synthesis was conducted by injecting 1 ml of precursor X and different volumes of precursor Y into the antisolvent toluene with vortexing at ~3400 RPM. **c** Colloidal $CsPbBr_3$ nanoplatelets and Mn-doped mixed-halide perovskites with increasing concentrations of the Mn-H_2O precursor, and **d** their corresponding drop-cast films. **e** Schematic representation of the Mn-doped $CsPbCl_yBr_{3-y}$ crystal lattice.

To obtain the Mn-doped perovskite samples, microliter quantities of precursor Y were injected into the toluene along with precursor X. Starting with 20 µL of precursor Y and 1 ml of precursor X, light magenta/purple PL was observed within 5 s, indicating the formation of a phase other than the initial blue-emitting $CsPbBr_3$. Mn-doped halide perovskites have been well-studied, and recent work suggests that Mn doping at a sufficiently high concentration leads to yellowish-orange PL

from the Mn d-d transition. Other studies have shown that lower Mn-doping levels generate pinkish-purple PL[36], which is in line with the observations from the present study when 20 μL of precursor Y was used.

To explore the possibility of obtaining stronger PL from Mn-doped halide perovskites, the quantity of the Mn-H_2O precursor was increased while maintaining the same volume of precursor X. As expected, following the injection of 40 μL of precursor Y, weak orange PL emissions were observed. With further increases in precursor Y, the colloidal solution continued to exhibit brighter emissions. With 100 μL of precursor Y, the colloidal solution exhibited intense PL emissions at ~611 nm, which was in strong agreement with past research on Mn-doped halide perovskites[37]. **Figure 1b** present the colloidal solutions and corresponding film samples for the Mn-doped mixed halides with an increase in the quantity of Mn-H_2O (0 – 100 μL), exhibited blue to orange PL over this range. To understand the effect of an excess quantity of precursor Y, its injection volume was increased at intervals of 20 μL. At 120 μL and 140 μL, the PL intensity from Mn (~611 nm) was noticeably lower (**Supporting Fig. S1**). In our analysis, 100 μL quantity of precursor Y was found to be optimal for the synthesis of Mn-doped mixed-halide perovskites exhibiting intense orange PL emissions. A schematic illustration of the crystal lattice for Mn-doped $CsPbCl_xBr_{1-x}$ is presented in **Fig. 1c**. Due to the presence of the Cl^- and Mn^{2+} ions, mixed-halide $[MnX_6]^{4-}$ octahedra formed in which Mn^{2+} acted as a B-site dopant by replacing the Pb^{2+} in $[PbX_6]^{4-}$.

To assess the physical morphology, TEM analysis of the samples (0 to 100 μL) was conducted (**Figs. 2a-e**). Initially, with 0 μL of precursor Y, $CsPbBr_3$ consisted of nanoplatelets with a size of ~50 nm. With injection of 20 μL of precursor Y, the $CsPbBr_3$ shifted to a mixture of irregular nonhomogeneous shapes, including platelets, cubes, rods, and their intermediates. Interestingly, at 40 μL, the sample exhibited a highly uniform morphology of nanocubes. With 60 μL of the Mn-

H_2O precursor, smaller cubes were observed. It appears these cubes were in the process of transforming into a nanowire-like morphology via a self-assembly process[38]. Finally, with 100 µL of the Mn-H_2O precursor, nanowires with a length of up to a few hundred nanometres were observed.

At this stage, it was possible that the material could be either $CsPbCl_3$ doped with Mn ions or mixed-halide perovskite $CsPbCl_xBr_{1-x}$ with Mn^{2+} at the B site replacing Pb. To understand the phase change that occurred after the injection of the Mn-H_2O precursor, all of the samples were analysed using XRD (**Supporting Fig. S2**). The XRD results revealed a continuous red shift with increasing volumes of the Mn-H_2O precursor injection, which was indicative of a phase transition towards a $CsPbCl_3$ perovskite lattice[39]. This was expected to be a result of mixed-halide phase formation because the Mn-H_2O precursor contained Cl^- and Mn^{2+} ions which are smaller compared to Br^- and Pb^{2+} ions. Here, Mn^{2+} replace the Pb^{2+} at the B site, leading to lattice contraction and resulting a red shift in the XRD peaks[40].

Optical properties of the samples are presented in **Figs. 2g and h**. Generally, Mn dopants exhibit PL characteristics independently of the composition of the host halide[41]. Using UV-vis analysis we observed that there was a continuous blue shift in absorption with injection of higher quantities of the precursor Y (**Supporting Fig. S3**). Initially, $CsPbBr_3$ had a maximum absorption peak at 445 nm, which was found to vary with respect to the injection quantities of precursor Y **(Fig. 2g)**. With 100 µL of precursor Y, the maximum absorption peak was found to shift by ~51 nm, reaching 394 nm. This strongly indicates the formation of a mixed-halide lattice with the incorporation of Cl^- ions, supporting our previous analysis. In accordance with the absorption spectra, a blue shift of ~50 nm was also observed in the host lattice PL (**Fig. 2h**). During our

analysis we observed that Mn PL peak position remained unchanged, though its intensity increased with higher injection quantity of the precursor Y.

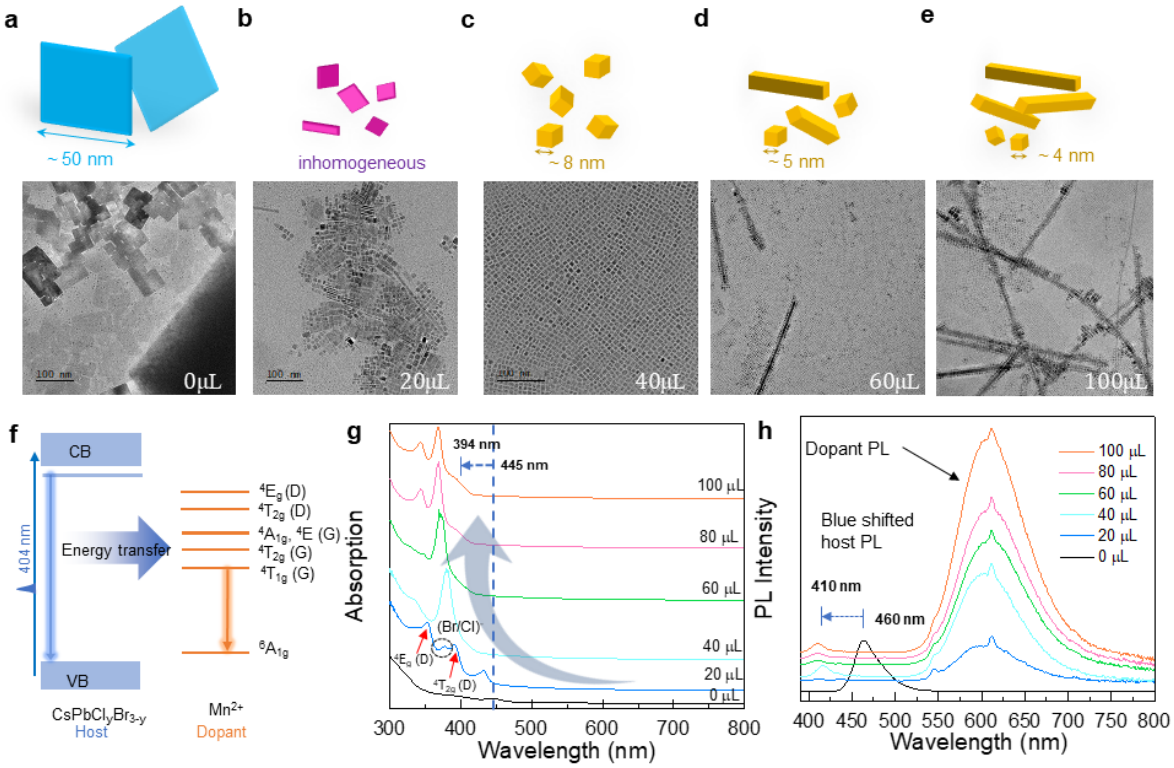

Fig. 2 TEM images of samples prepared with different concentrations of the Mn-H_2O precursor: **a** 0, **b** 20, **c** 40, **d** 60, and **e** 100 μL. Upon injection of 20 μL precursor, $CsPbBr_3$ nanosheets start to transform into smaller irregular shapes. c, 40 μL injection transforms them into nano cubes. d, 60 μL makes even smaller cubes and starts formation of nanowires. e, at 100 μL of Mn-H_2O injection they further transform into nanowires. **f** Model of the possible mechanisms for host-to-dopant energy transfer in Mn-doped mixed-halide perovskites. The host lattice exhibits PL emissions at ~ 410 nm. The Mn^{2+} dopant has PL emissions centered at ~611 nm. The energy levels for octahedrally coordinated Mn^{2+} ions in the $CsPbCl_yBr_{3-y}$ host lattice are shown. **g** Absorption and **h** PL spectra of samples 0 - 5 prepared using 0, 20, 40, 60, 80, and 100 μL of the Mn-H_2O precursor. The sharp absorption peaks appearing with 20 μL of Mn-H_2O are assigned as ^4E_g(D)

and $^4T_{2g}$(D) in accordance with crystal field theory and the T-S diagram for Mn^{2+}. The small absorption peak denoted by the dotted circle may be the result of mixed halides intermediates.

We observed the appearance of a broad peak covering 560 nm to 650 nm emitting an orange PL which was generally observed for octahedrally coordinated Mn^{2+} [42]. It was hypothesized that the Mn ions were located at the B site after replacing Pb. It has been widely reported that, for B-site-positioned Mn ions, PL is usually observed at 570–650 nm. On the other hand, with interstitial doping, the Mn PL exhibits a significant red shift to 650–700 nm[43]. Based on the crystal field theory, and Tanabe-Sugano (T-S) diagram[44], a model depicting the energy level of octahedrally coordinated Mn^{2+} and possible host-to-dopant energy transfer mechanisms was constructed (**Fig. 2f**).

As shown in **Fig. 2g**, two intense absorption peaks emerged with the injection of 20 µL of precursor Y. These peaks were more intense than that of the host lattice absorption. According to the T-S model, these absorption peaks were closely correlated with the absorption peaks of octahedrally coordinated Mn^{2+} [45]. Similarly, with the addition of precursor Y, the doped host lattice PL was considerably lower compared to the undoped host lattice, indicating efficient charge transfer from the host to the dopant[46]. In our analysis, the dopant Mn^{2+} PL had a higher intensity than the host lattice PL. During the physical transition from an undoped to a doped lattice, the only variable was the addition of precursor Y, which introduced Mn^{2+} ions, Cl^- ions, and H_2O molecules to the colloidal $CsPbBr_3$ system. Cl^- ions influence the system via the formation of the $CsPbCl_xBr_{1-x}$ lattice, while H_2O molecules may act as ligands by stripping OA^- and OAM^+, which was confirmed with FTIR (**Supporting Fig. S4**). We compared FTIR spectra of samples prepared with different quantities of precursor Y. Both the samples showed identical spectra while sample

prepared with 100 μL of water-based precursor Y exhibited much broader O-H peak at 3344 cm^{-} than that of sample prepared with 20 μL of precursor Y. Generally, broad O-H peak around 3344 cm^{-} denotes the presence of water molecules in colloidal systems[47]. Because water is amphiprotic in nature, two water molecules can react with each other while undergoing in an autoionization process to form OH^- and H_3O^+ ions as per following reaction: $2H_2O \rightarrow H_3O^+ + OH^-$

These ions formed by self-ionization of H_2O molecules can potentially strip and replace OA^- and OLA^+ ligands from the perovskite NC surfaces. During this process, NCs could undergo morphological transformation along with doping of manganese ions.

To gain more insight into the PL mechanisms underlying Mn-doped mixed-halide NCs, temperature-dependent PL analysis of the sample prepared with 100 μL of Mn-H_2O was conducted. For analysis, a drop-cast film prepared using 300 μL of this colloidal solution was used. In **Fig. 3a**, PL spectra of excitons and Mn^{2+} doped levels of Mn:$CsPbCl_xBr_{1-x}$ perovskite nanowires were measured for increasing temperature from 6 K up to 300 K. The emission of excitons is weak compared to that of Mn^{2+} doped levels, which can be attributed to an energy transfer from exciton to Mn^{2+} doped levels[48,49,50]. Additionally, both exciton and Mn^{2+} emission show blue shift with increasing temperature (**Fig. 3a)**. In **Fig. 3b**, temperature dependent peak energy of excitons and Mn^{2+} doped levels were obtained. While temperature increases from 6 K up to 300 K, excitons (~25 meV) and Mn^{2+} doped levels (~41 meV) show a similar energy shift. In the case of the excitons in perovskites, the temperature dependent blueshift can be explained by the competition of lattice expansion and electron-phonon interaction [48,49,51] . On the other hand, Mn^{2+} doped levels depend on the crystal field splitting. With increasing temperature, the lattice expansion in $CsPbCl_xBr_{1-x}$ perovskites was known to decrease the crystal field strength, resulting in a blueshift[48,49].

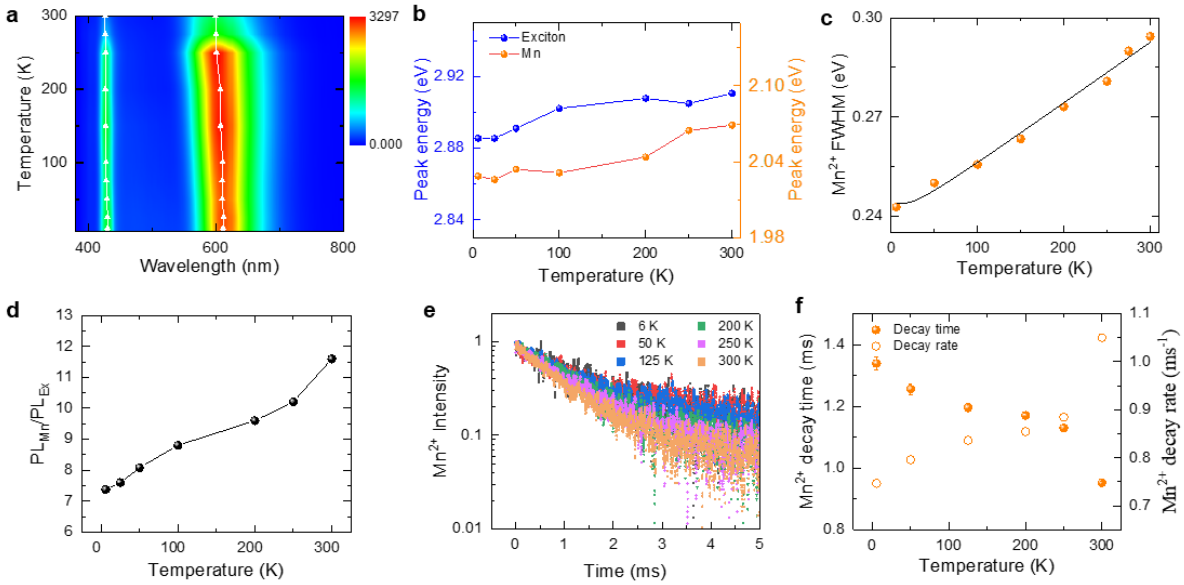

Fig. 3 a For increasing temperature from 6 K up to 300 K, PL spectrum of free excitons and Mn^{2+} doped levels were measured from Mn:$CsPbCl_yBr_{3-y}$ perovskite nanowires, which were formed by the condition of X:Y (1 ml: 100 μL). **b** Temperature dependent peak energy shift of excitons and Mn^{2+} doped levels. **c** Integrated PL intensity ratio of Mn^{2+} doped levels to free excitons. **d** Linewidth of Mn^{2+} doped levels for temperature, where experimental results (orange dots) were compared with Eq. (1) (black line). **e** Time-resolved PL of Mn^{2+} doped levels for temperature under excitation of 405 nm. **f** PL decay time of Mn^{2+} doped levels for temperature.

As shown in **Fig. 3c**, the linewidth of Mn^{2+} doped levels become broadened for increasing temperature. In general, temperature dependence of linewidth broadening is explained by electron-phonon interaction[52,53]. Recently, the exciton PL linewidth of Mn:$CsPbCl_3$ perovskites was measured for increasing temperature from 80 K to 400 K[53], where acoustic phonon interaction becomes dominant up to 200 K, resulting in a linear temperature dependence, but optical phonon interaction becomes significant for increasing temperature over 200 K. However, temperature dependent linewidth broadening of Mn^{2+} doped levels in mixed halide perovskite $CsPbCl_xBr_{1-x}$ is rarely known. We measured FWHM (fullwidth at half maximum) Γ(T) of Mn^{2+} doped levels with

increasing temperature from 6 K up to 300 K (**Supporting Fig. S5)**, and the result was compared with Eq. (1) [53],

$$\Gamma(T) = \Gamma_0 + \alpha T + \frac{\beta}{e^{\hbar\omega_{LO}/k_B T} - 1} \qquad (1)$$

, whereby temperature independent inhomogeneous linewidth Γ_0 = 243.23 meV and coupling coefficients of acoustic ($\alpha = 90.8$ μeV) and optical phonon ($\beta = 24.6$ meV) were obtained with LO-phonon energy ($\hbar\omega_{LO} = 19$ meV)[54].

In **Fig. 3d**, integrated PL intensity of Mn^{2+} doped levels were normalized by that of excitons for increasing temperature, whereby the intensity ratio quantifies the competition between exciton recombination and Mn^{2+} doped level transition. While temperature increases from 6 K to 300 K, the ratio increases from 7.37 to 11.6. The enhanced ratio can be explained by increased energy transfer efficiency from exciton to Mn^{2+} doped levels[48,49,50]. As shown schematically in **Fig. 2f**, it was known that an energy transfer occurs from the exciton states of host $CsPbCl_xBr_{1-x}$ to the Mn^{2+} doped levels, where the transition of $^4T_1 \rightarrow {}^6A_1$ dominates. Therefore, the exciton PL lifetime of $CsPbCl_xBr_{1-x}$ becomes shortened compared to that of undoped $CsPbCl_xBr_{1-x}$. However, the energy transfer efficiency is sensitive to temperature and competes with the exciton decay time of host $CsPbCl_xBr_{1-x}$. The PL decay time of excitons (~ a few ns) at low temperatures (< 10 K) was known to be rapid compared to the energy transfer time, but gradually slows down for increasing temperature. As a result, the energy transfer to Mn^{2+} doped levels become efficient, leading to an enhancement of the PL intensity of Mn^{2+} doped levels for increasing temperature[49,50].

On the other hand, the optical transitions of Mn^{2+} doped levels also need to be investigated in terms of temperature dependence. In **Fig. 3e**, time-resolved PL of Mn^{2+} doped levels were measured near 600 nm for increasing temperature, which corresponds to the dominant $^4T_1 \rightarrow {}^6A_1$

transition. Because the *d-d* transition of Mn^{2+}ions was known to be spin and parity-forbidden, the monotonic PL decay of $^4T_1 \rightarrow {}^6A_1$ proceeds slowly in milliseconds. The mono-exponential decay characteristic indicates that only one type of luminescent centre (Mn^{2+}) is associated, and that Mn^{2+} ions are placed in a homogeneous crystal field environment[50]. While temperature increases up to 300 K, the monotonic PL decay time becomes shortened due to thermal quenching [49,50,55]. In **Fig. 3f**, both PL decay time and decay rate of Mn^{2+} doped levels were plotted for temperature. However, the change is not significant while temperature increases from 6 K to 300 K. Therefore, the energy transfer to Mn^{2+} doped levels is mainly governed by the decay time of excitons in $CsPbCl_xBr_{1-x}$ host.

The quantity of Mn^{2+} ions incorporated into the mixed-halide perovskite lattice was analysed using inductively coupled plasma mass spectroscopy (ICP-MS, **Supporting Fig. S6**). It was confirmed that the samples prepared with different quantities of the precursor had different amounts of Mn incorporated into the perovskite NCs. The sample prepared with 20 μL of the Mn-H2O precursor had a Mn content of 0.14 wt.%, compared with 3.34 wt.% for the sample prepared with 100 μL of the precursor. These results thus supported the observation of enhanced PL with higher volumes of the Mn-H_2O precursor shown in **Fig. 2h**.

Water and toluene are virtually immiscible due to the large difference in relative solvent polarity[35]. Therefore, the injected precursor Y can sink at the bottom of the perovskite colloidal solution even after forming the Mn^{2+} doped mixed halide perovskite. In order to check this, we kept the as-synthesized colloidal solution in an ambient exposure without separating the injected precursor Y. After 5 days, the colloidal solution became dark in appearance but still exhibited orange luminescence under UV excitation. We analysed and compared optical properties of a newly prepared sample, named “neat” and the aged sample named “dark” in **Supporting Fig. S7.**

UV-VIS spectra revealed that sharp the absorption peak observed from the neat sample became smaller in the dark sample **(Supporting Fig. S7a)**. Interestingly, the dark sample exhibited a small blue-shift and relatively lower intensity of host lattice PL. Also, it exhibited relatively lower PL intensity originating from dopant Mn^{2+} compared to that of the neat sample. **(Supporting Fig. S7b)**. Dark appearance of the aged sample may originate from the formation of amine oxide denoted as $R_3N^+ \rightarrow O^-$. We presume that stripped oleylamine by self-ionisation of water molecules may be available in the colloidal solution. In the presence of H_2O, it could undergo oxidation reaction resulting in the formation of amine oxide and causing darker appearance[56].

To further improve PL emission, we employed an inorganic passivation strategy by using hydrohalic acids, HBr and HCl, on the sample (precursor Y: 100 μL). Different quantities of HCl and HBr were injected along with precursors X and Y, and their effects on optical properties were studied. **Supporting Fig. S8** presents the optical images of the resulting solutions. In the presence of HCl, the Mn PL intensity was enhanced without changing its orange PL emission peak position (**Supporting Fig. S8a)**. However, the addition of HBr led to intense blue PL (**Supporting Fig. S8b)**.

The optical properties are analysed in more detail in **Supporting Fig. S9**. With the addition of HCl, there was no change in the Mn PL peak position for any HCl quantity (**Supporting Fig. S9a)**, but the absorption exhibited a blue shift by a few nanometres (**Supporting Fig. S9b)**. Interestingly, with an increase in HBr injection, absorption was redshifted (**Supporting Fig. S9c)**, the PL from Mn weakened, giving rise to intense blue PL from the lattice (**Supporting Fig. S9d)**. This indicated that the Br ions replace Mn atoms in the lattice to form a stable $CsPbBr_3$ phase. In contrast, HCl acted in favour of the Mn ions and enhanced the PL[57].

To fully understand the effect of HBr and HCl on the optical properties of the mixed halides, excitation-dependent PL analysis of the samples prepared with different quantities of HCl and HBr was carried out (**Supporting Fig. S10**).

The sample prepared with 10 μL of HBr showed no change in the PL intensity irrespective of the excitation wavelength (**Supporting Fig. S10a**). However, at an excitation of 420 nm, a small peak (indicated by an arrow) appeared near the host lattice PL, which could be indicative of efficient Br-based host lattice radiative transition. Here, the PL intensity from the Mn peak remained unchanged. With 10 μL of HCL, the Mn PL intensity was relatively similar at an excitation of 365 nm and 400 nm, but it fell dramatically at an excitation of 420 nm (**Supporting Fig. S10b**). This is associated with the mixed-halide host lattice transition towards $CsPbCl_3$ due to the excess Cl^- ions from the addition of HCl. Because $CsPbCl_3$ has a wider band gap than $CsPbBr_3$, it cannot readily absorb an excitation wavelength of 420 nm, thus reducing the PL. This mechanism was later confirmed with the addition of 20 μL of HCl (**Fig. S10d**).

The addition of 20 μL of HBr drastically lowered the PL originating from Mn^{2+} **Supporting Fig. S10c**. It indicated that the addition of Br^- ions reduced the overall PL intensity from Mn, while the addition of Cl^- ions enhanced this PL.[58]

Further, PLQY of the samples prepared with different quantities of HCl was analysed (**Supporting Fig. S11a**). It was found that the PLQY was enhanced initially with an increase in HCl. However, at more than 20 μL HCL, the PLQY decreased, and this may be due to the excess acid damaging the NC surface. The sample prepared with 20 μL of HCl thus exhibited the highest PLQY of 69.11% and was selected for stability testing. A colloidal solution of this sample exhibited ~ 100% of its initial PL for up to 1 year when stored even under ambient conditions (**Supporting**

Fig. S11b). Due to the excellent PLQY and outstanding stability of this sample, we decided to evaluate its thermal performance. Under continuous heating and cooling cycles from 21 °C to 120 °C (**Fig. 4a**).

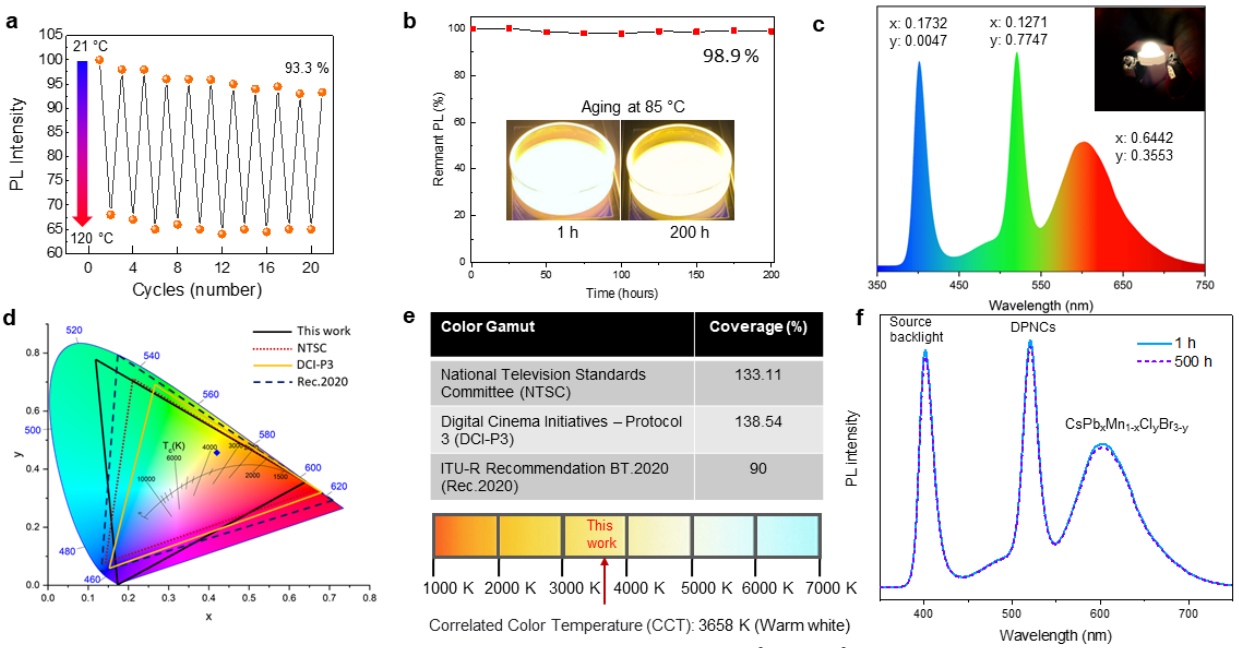

Fig. 4 **a** Normalized PL intensity plots of sample prepared using 20 µL of HCl at thermal cycling between 21 °C and 120 °C. After 20 consecutive cycles, the sample retained 93.3% of initial PL. **b** Thermal performance of the same sample during continuous heating at 85 °C with PL retention of 98.9%. **c** PL spectra of LED prepared using combination of green emitting DPNCs and Mn doped sample synthesized with 20 µL of HCl as an active layer on blue UV chip. Operating LED is shown in inset picture. Commission internationale de l'éclairage (CIE) x, y coordinates are shown on the top of corresponding PL emission. **d** Gamut coverage of our LED is shown on 1931 CIE diagram compared with industry standard NTSC, DCI-P3 and Rec. 2020 color gamut. **e** A comparison table prepared using values extracted from (d) shows our LED exhibiting gamut coverage of 133.11%, 138.54%, and 90% of NTSC, DCI-P3, and Rec.2020 gamut respectively with CCT of 3658 K. **f** Operating stability of our LED device. It exhibited negligible PL reduction after 500 h of continuous operation.

At 120 °C, its PL quenched to 66% of the original PL intensity and after 20 cycles, the sample retained 93% of its original PL intensity when cooled down to 21 °C. In general, commercially available phosphor materials are benchmarked at 85 °C heating[59]. Thus, we followed the same testing method, and it was found that our sample retained 98.9% of the original PL intensity after 200 h of continuous heating at 85 °C (**Fig. 4b**). These results indicated the true potential of our phosphor for commercial use.

Based on these results, we fabricated an LED by combining this material as an orange-red emitting source along with green emitting DPNCs prepared as per our previous report along with 400 nm UV chip as a blue source[33]. **Figure 4c** presents spectra of the LED that produces warm white light (the inset shows the photograph of an operating device). Spectral coverage of our LED is shown in **Fig. 4d**. It exhibited 133.11 % coverage of NTSC, 138.54 % of DCI-P3 and 90 % of Rec.2020 colour gamut. With CCT of 3658 k our LED could fulfil the need for warm white studio lighting and backlit displays (**Fig. 4e**). The operational stability of our device is shown in **Fig. 4f**. Fortunately, our device exhibited negligible degradation under continuous operation for 500 h.

Conclusion

In summary, the water-facilitated ultrafast formation of highly luminescent Mn-doped mixed-halide perovskites at room temperature was successfully demonstrated in the present study, with water acting as a supersaturated precursor providing Mn^{2+} dopant without being mixed in the antisolvent during the synthesis process. Via self-ionization, water played role of an inorganic passivator for the NCs surface. The resulting sample exhibited bright orange PL (~ 611 nm) with

the incorporation of Mn^{2+}. As a function of dopant precursor injection, the NC morphology evolved from nanoplatelets to nanocubes and then to nanowires.

The effect of HCl and HBr on Mn incorporation was also assessed. The sample prepared with 20 μL of HCl exhibited a high PLQY of 69.11% and remained stable for up to 1 year. Using this sample in combination with green-emitting DPNCs and a backlit UV chip, a highly stable LED was fabricated, exhibiting warm white light with the CIE coordinates x = 0.4198, y = 0.4569. It covered 133.11% of NTSC, 138.54% of DCI-P3 and 90% of Rec.2020 colour gamut with a CCT of 3658 k. The unique method proposed in this study delivers Mn-doped halide perovskites with interesting photophysical properties and device grade orange-red emitting perovskite phosphor material to be used for warm white lighting applications. We believe this method could be extended to the non-volatile doping and incorporation of various elements into halide perovskite lattices.

References

1. Dey, A. et al. State of the art and prospects for halide perovskite nanocrystals. *ACS nano* **15**, 10775-10981 (2021). https://doi.org/10.1021/acsnano.0c08903

2. Otero-Martínez, C. et al. Fast A-Site Cation Cross-Exchange at Room Temperature: Single-to Double- and Triple-Cation Halide Perovskite Nanocrystals. *Angew. Chem., Int. Ed.* **61**, 202205617 (2022). https://doi.org/10.1002/anie.202205617

3. Kim, J. S., et al. Ultra-bright, efficient and stable perovskite light-emitting diodes. *Nature* **611**, 688-694 (2022). https://doi.org/10.1038/s41586-022-05304-w

4. McMeekin, D. P. et al. Intermediate-phase engineering via dimethylammonium cation additive for stable perovskite solar cells. *Nat. Mater.* **22**, 73-83 (2023). https://doi.org/10.1038/s41563-022-01399-8

5. Zaffalon, M. L. et al. Extreme γ-ray radiation hardness and high scintillation yield in perovskite nanocrystals. *Nat. Photonics* **16**, 860-868 (2022). https://doi.org/10.1038/s41566-022-01103-x

6. Cho, S. et al. Hybridisation of perovskite nanocrystals with organic molecules for highly efficient liquid scintillators. *Light: Sci. Appl.* **9**, 156 (2020). https://doi.org/10.1038/s41377-020-00391-8

7. Yen, M.-C. et al. All-inorganic perovskite quantum dot light-emitting memories. *Nat. Commun.* **12**, 4460 (2021). https://doi.org/10.1038/s41467-021-24762-w

8. Ma, X. et al. Doping in inorganic perovskite for photovoltaic application. *Nano Energy* **78**, 105354 (2020). https://doi.org/10.1016/j.nanoen.2020.105354

9. Mocatta, D. et al. Heavily doped semiconductor nanocrystal quantum dots. *Science* **332**, 77-81 (2011). https://doi.org/10.1126/science.1196321

10. Pradhan, N. Mn-doped semiconductor nanocrystals: 25 years and beyond. *J. Phys. Chem. Lett.* 10, 2574-2577 (2019). https://doi.org/10.1021/acs.jpclett.9b01107

11. Erwin, S. C. et al. Doping semiconductor nanocrystals. *Nature* **436**, 91-94 (2005). https://doi.org/10.1038/nature03832

12. Long, G. et al. Carrier-dopant exchange interactions in Mn-doped PbS colloidal quantum dots. *Appl. Phys. Lett.* **101**, 062410 (2012). https://doi.org/10.1063/1.4743010

13. Zhang, H. et al. An aqueous route synthesis of transition-metal-ions-doped quantum dots by bimetallic cluster building blocks. *J. Am. Chem. Soc.* **142**, 16177-16181 (2020). https://doi.org/10.1021/jacs.0c07274

14. Yang, H., Santra, S. & Holloway, P. H. Syntheses and applications of Mn-doped II-VI semiconductor nanocrystals. *J. Nanosci. Nanotechnol.* **5**, 1364-1375 (2005). https://doi.org/10.1166/jnn.2005.308

15. Pradhan, N. & Xiaogang, P. Efficient and color-tunable Mn-doped ZnSe nanocrystal emitters: control of optical performance via greener synthetic chemistry. *J. Am. Chem. Soc.* **129**, 3339-3347 (2007). https://doi.org/10.1021/ja068360v

16. Mir, W. J., Jagadeeswararao, M., Das, S. & Nag, A. Colloidal Mn-doped cesium lead halide perovskite nanoplatelets. *ACS Energy Lett.* **2**, 537-543 (2017). https://doi.org/10.1021/acsenergylett.6b00741

17. Lin, C.-C. et al. Spin-polarized photocatalytic CO_2 reduction of Mn-doped perovskite nanoplates. *J. Am. Chem. Soc.* **144**, 15718-15726 (2022). https://doi.org/10.1021/jacs.2c06060

18. Liu, H. et al. $CsPb_xMn_{1-x}Cl_3$ perovskite quantum dots with high Mn substitution ratio. *ACS Nano* **11**, 2239-2247 (2017). https://doi.org/10.1021/acsnano.6b08747

19. Chen, X. et al. Substantial Improvement of Operating Stability by Strengthening Metal-Halogen Bonds in Halide Perovskites. *Adv. Funct. Mater.* **32**, 2112129 (2022). https://doi.org/10.1002/adfm.202112129

20. Wang, Y., Chen, Y., Zhang, T., Wang, X. & Zhao, Y. Chemically Stable Black Phase $CsPbI_3$ Inorganic Perovskites for High-Efficiency Photovoltaics. *Adv. Mater.* **32**, 2001025 (2020). https://doi.org/10.1002/adma.202001025

21. Li, D. et al. Ultraefficient singlet oxygen generation from manganese-doped cesium lead chloride perovskite quantum dots. *ACS Nano* **14**, 12596-12604 (2020). https://doi.org/10.1021/acsnano.0c04181

22. Hou, L. et al. Synthesis of Gram-Scale Ultrastable Mn-Doped 2D Perovskites for Light-Emitting Diodes. *Adv. Mater. Interfaces* **8**, 2002175 (2021). https://doi.org/10.1002/admi.202002175

23. Hou, S., Gangishetty, M. K., Quan, Q. & Congreve, D. N. Efficient blue and white perovskite light-emitting diodes via manganese doping. *Joule* **2**, 2421-2433 (2018). https://doi.org/10.1016/j.joule.2018.08.005

24. Bai, X. et al. In situ preparation of Mn-doped perovskite nanocrystalline films and application to white light emitting devices. *J. Colloid Interface Sci.* **606**, 1163-1169 (2022). https://doi.org/10.1016/j.jcis.2021.08.068

25. Hou, L., Zhu, Y., Zhu, J., Gonga Y. & Li C. Mn-doped 2D Sn-based perovskites with energy transfer from self-trapped excitons to dopants for warm white light-emitting diodes. *J. Mater. Chem. C* **8**, 8502-8506, (2020). https://doi.org/10.1039/D0TC00959H

26. Han, L. et al. Boosted luminescence efficiency and stability of Mn-doped perovskite nanoplatelets via incorporating Cd^{2+} ions. *Mater. Res. Bull.* **151**, 111825 (2022). https://doi.org/10.1016/j.materresbull.2022.111825

27. Otero-Martínez, C., Fiuza-Maneiro, N. & Polavarapu L. Enhancing the Intrinsic and Extrinsic Stability of Halide Perovskite Nanocrystals for Efficient and Durable Optoelectronics. *ACS Appl. Mater. Interfaces* 14, 34291-34302 (2022). https://doi.org/10.1021/acsami.2c01822

28. Chen, B., Wang, S., Song, Y., Li, C. & Hao F. A critical review on the moisture stability of halide perovskite films and solar cells. *J. Chem. Eng.* **430**, 132701 (2022). https://doi.org/10.1016/j.cej.2021.132701

29. Liu, K. et al. Moisture-triggered fast crystallization enables efficient and stable perovskite solar cells. *Nat. Commun.* **13**, 4891 (2022). https://doi.org/10.1038/s41467-022-32482-y

30. Li, X. et al. Highly stable $CsPbBr_3$ quantum dots by silica-coating and ligand modification for white light-emitting diodes and visible light communication. *J. Chem. Eng.* **419**, 129551 (2021). https://doi.org/10.1016/j.cej.2021.129551

31. Zhong, Q. et al. One-pot synthesis of highly stable $CsPbBr_3@SiO_2$ core–shell nanoparticles. *ACS Nano* **12**, 8579-8587 (2018). https://doi.org/10.1021/acsnano.8b04209

32. Rossi, C. et al. Exploiting the transformative features of metal halides for the synthesis of $CsPbBr_3@SiO_2$ core–shell nanocrystals. *Chem. Mater.* **34**, 405-413 (2021). https://doi.org/10.1021/acs.chemmater.1c03749

33. Fulari, A. V. et al. Precursor silanization assisted synthesis and optical tuning of dual-phase perovskite nanocrystals embedded in silica matrix with high environmental stability. *J. Colloid Interface Sci.* **630**, 212-222 (2023). https://doi.org/10.1016/j.jcis.2022.10.012

34. Hassan, Y. et al. Facile synthesis of stable and highly luminescent methylammonium lead halide nanocrystals for efficient light emitting devices. *J. Am. Chem. Soc.* **141**, 1269-1279 (2019). https://doi.org/10.1021/jacs.8b09706

35. https://sites.google.com/site/miller00828/in/solvent-polarity-table

36. Luo, B. et al. B-Site doped lead halide perovskites: synthesis, band engineering, photophysics, and light emission applications. *J. Mater. Chem. C* **7**, 2781-2808 (2019). https://doi.org/10.1039/C8TC05741A

37. De, A., Mondal, N. & Samanta. A. Luminescence tuning and exciton dynamics of Mn-doped $CsPbCl_3$ nanocrystals. *Nanoscale* **9**, 16722-16727 (2017). https://doi.org/10.1039/C7NR06745C

38. Tong, Y. et al. From precursor powders to $CsPbX_3$ perovskite nanowires: one-pot synthesis, growth mechanism, and oriented self-assembly. *Angew. Chem., Int. Ed.* **56**, 13887-13892 (2017). https://doi.org/10.1002/anie.201707224

39. Protesescu, L. et al. Nanocrystals of cesium lead halide perovskites ($CsPbX_3$, X= Cl, Br, and I): novel optoelectronic materials showing bright emission with wide color gamut. *Nano Lett.* **15**, 3692-3696 (2015). https://doi.org/10.1021/nl5048779

40. Torma, A. J. et al. Interstitial nature of Mn^{2+} doping in 2D perovskites. *ACS Nano* **15**, 20550-20561 (2021). https://doi.org/10.1021/acsnano.1c09142

41. Mir, W. J. et al. Postsynthesis doping of Mn and Yb into $CsPbX_3$ (X= Cl, Br, or I) perovskite nanocrystals for down conversion emission. *Chem. Mater.* **30**, 8170-8178 (2018). ttps://doi.org/10.1021/acs.chemmater.8b03066

42. Han, P. et al. Manganese-doped, lead-free double perovskite nanocrystals for bright orange-red emission. *ACS Cent. Sci.* **6**, 566-572 4 (2020). https://doi.org/10.1021/acscentsci.0c00056

43. Li, Z.-J. et al. Complete dopant substitution by spinodal decomposition in Mn-doped two-dimensional $CsPbCl_3$ nanoplatelets. *Chem. Mater.* **30**, 6400-6409 (2018). https://doi.org/10.1021/acs.chemmater.8b02657

44. Tanabe, Y. & Sugano, S. On the Absorption Spectra of Complex Ions, III The Calculation of the Crystalline Field Strength. *J. Phys. Soc. Jpn.* **1**, 864–877 (1956). https://doi.org/10.1143/JPSJ.11.864

45. Almutlaq, J. et al. $CsMnBr_3$: Lead-free nanocrystals with high photoluminescence quantum yield and picosecond radiative lifetime. *ACS Materials Lett.* **3**, 290-297 (2021). https://doi.org/10.1021/acsmaterialslett.0c00603

46. Rossi, D., Parobek, D., Dong, Y. & Son, D. H. Dynamics of exciton–Mn energy transfer in Mn-doped $CsPbCl_3$ perovskite nanocrystals. *J. Phys. Chem. C* **121**, 17143-17149 (2017). https://doi.org/10.1021/acs.jpcc.7b06182

47. Müller, C. et al. Water infiltration in methylammonium lead iodide perovskite: Fast and inconspicuous. *Chem. Mater.* **27**, 7835-7841 (2015). https://doi.org/10.1021/acs.chemmater.5b03883

48. Xu, K. & Xu, K. Tuning exciton-Mn^{2+} energy transfer in mixed halide perovskite nanocrystals. *Chem. Mater.* **30,** 5346-5352 (2018). https://doi.org/10.1021/acs.chemmater.8b02157

49. Yuan, X. et al. Photoluminescence temperature dependence, dynamics, and quantum efficiencies in Mn^{2+}-doped $CsPbCl_3$ perovskite nanocrystals with varied dopant concentration. *Chem. Mater.* **29**, 8003-8011 (2017). https://doi.org/10.1021/acs.chemmater.7b03311

50. Fei, L. et al. Enhanced luminescence and energy transfer in Mn^{2+}-doped $CsPbCl_{3-x}Br_x$ perovskite nanocrystals. *Nanoscale* **10**, 19435-19442 (2018). https://doi.org/10.1039/C8NR05492D

51. Wu, W., Liu, W., Wang, Q., Han, Q. & Yang, Q. Temperature-dependent photoluminescence of pure and Mn-doped $CsPbBr_3$ nanocrystals. *J. Alloys Compd.* **787**, 165-172 (2019). https://doi.org/10.1016/j.jallcom.2019.02.032

52. Xing, Y. et al. Temperature-dependent photoluminescence of Mn-doped $CsPbCl_3$ perovskite nanocrystals in mesoporous silica. *J. Lumin.* **204**, 10-15 (2018). https://doi.org/10.1016/j.jlumin.2018.07.029

53. Naresh, V., Cho, M.-K., Cha, P.-R. & Lee, N. Polar- solvent free sonochemical synthesis of Mn(II)-doped $CsPbCl_3$ perovskite nanocrystals for dual-color emission. *ACS Appl. Nano Mater.* **6**, 4693-4706 (2023). https://doi.org/10.1021/acsanm.3c00182

54. Pashuk, I. P., Pidzyrajlo, N. S. & Matsko, M. G. Exciton absorption, luminescence and resonance raman scattering in $CsPbCl_3$ and $CsPbBr_3$ crystals at low temperature. *Sov. Phys. Sol. State*. **23**, 1263-1266 (1981).

55. Xing, K, et al. Improved doping and emission efficiencies of Mn-doped $CsPbCl_3$ perovskite nanocrystals via nickel chloride. *J. Phys. Chem. Lett.* **10**, 4177-4184 (2019). https://doi.org/10.1021/acs.jpclett.9b01588

56. Murahashi, S.-I. & Imada, Y. Amine oxidation. *Transition Metals for Organic Synthesis: Building Blocks and Fine Chemicals* 36, 497-507 (2004). https://doi.org/10.1002/9783527619405.ch5o

57. Das Adhikari, S., Dutta, S. K., Dutta, A., Guria, A. K. & Pradhan, N. Chemically tailoring the dopant emission in manganese-doped $CsPbCl_3$ perovskite nanocrystals. *Angew. Chem., Int. Ed.* **56**, 8746-8750 (2017). https://doi.org/10.1002/anie.201703863

58. Ha, S. K., Shcherbakov-Wu, W., Powers, E. R., Paritmongkol, W. & Tisdale, W. A. Power-dependent photoluminescence efficiency in manganese-doped 2D hybrid perovskite nanoplatelets. *ACS Nano* **15**, 20527-20538 (2021). https://doi.org/10.1021/acsnano.1c09103

59. He, Q., Mei, E., Liang, X. & Xiang W. Ultrastable PVB films-protected $CsPbBr_3/Cs_4PbBr_6$ perovskites with high color purity for nearing Rec. 2020 standard. *J. Chem. Eng.* **419**, 129529 (2021).